High Sensitivity of Diamond Resonant Microcantilevers for Direct Detection in Liquids As Probed by Molecular Electrostatic Surface Interactions

Alexandre Bongrain, Charles Agnès, Lionel Rousseau, Emmanuel Scorsone, Jean-Charles Arnault, Sébastien Ruffinatto, Franck Omnès, Pascal Mailley, Gaelle Bazin Lissorgues, Philippe Bergonzo

High Sensitivity of Diamond Resonant Microcantilevers for Direct Detection in Liquids As Probed by Molecular Electrostatic Surface Interactions

Alexandre Bongrain[*,1,2], Charles Agnès[1], Lionel Rousseau[2], Emmanuel Scorsone[1], Jean-Charles Arnault[1], Sébastien Ruffinato[3,4], Franck Omnès[3], Pascal Mailley[4], Gaëlle Lissorgues[2], Philippe Bergonzo[1]

[1]CEA, LIST, Diamond Sensors Laboratory, F-91191 Gif-sur-Yvette, France
[2]ESIEE ESYCOM University Paris Est, Cité Descartes, BP99, 93162 Noisy Le Grand, France
[3]Institut Neel, UPR CNRS 2940, 25 Rue des Martyrs, BP 166, F-38042 Grenoble, France
[4]CEA, INAC, SPrAM UMR 5819 (UJF, CNRS, CEA), F-38054 Grenoble, France
* Corresponding author

ABSTRACT

Resonant microcantilevers have demonstrated that they can play an important role in the detection of chemical and biological agents. Molecular interactions with target species on the mechanical microtransducers surface generally induce a change of the beam's bending stiffness, resulting in a shift of the resonance frequency. In most biochemical sensor applications, cantilevers must operate in liquid, even though damping deteriorates the vibrational performances of the transducers. Here we focus on diamond-based microcantilevers since their transducing properties surpass those of other materials. In fact, among a wide range of remarkable features, diamond possesses exceptional mechanical properties enabling the fabrication of cantilever beams with higher resonant frequencies and *Q*-factors than when made from other conventional materials. Therefore, they appear as one of the top-ranked materials for designing cantilevers operating in liquid media. In this study, we evaluate the resonator sensitivity performances of our diamond microcantilevers using grafted carboxylated alkyl chains as a tool to investigate the subtle changes of surface stiffness as induced by electrostatic interactions. Here, caproic acid was immobilized on the hydrogen-terminated surface of resonant polycrystalline diamond cantilevers using a novel one-step grafting technique that could be also adapted to several other functionalizations. By varying the pH of the solution one could tune the $-COO^-$ /– COOH ratio of carboxylic acid moieties immobilized on the surface, thus enabling fine variations of the surface stress. We were able to probe the cantilevers resonance frequency evolution and correlate it with the ratio of $-COO^-$ /– COOH terminations on the functionalized diamond surface and consequently the evolution of the electrostatic potential over the cantilever surface. The approach successfully enabled one to probe variations in cantilevers bending stiffness from several tens to hundreds of millinewtons/meter, thus opening the way for diamond microcantilevers to direct sensing applications in liquids. The evolution of the diamond surface chemistry was also investigated using X-ray photoelectron spectroscopy.

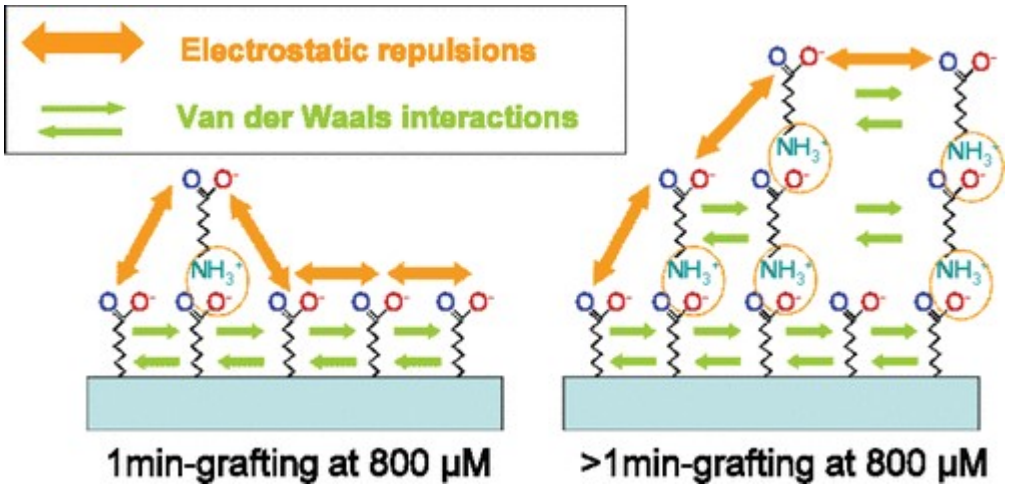

INTRODUCTION

Over the last years, microcantilevers used in static or oscillating regimes have demonstrated high efficiency for detection of chemical and biological compounds, including DNA sequences (1-3) antibodies (4), spores (5), bacteria (6), and viruses (7). Generally, the presence of target species over the transducer surface contributes to increase the cantilever effective mass and induces modification of the bending stiffness due to molecular interactions such as electrostatic repulsions, steric obstructions, van der Waals interactions, or hydration forces. Those contributions induce cantilever bending and cantilever resonance frequency shifts that are monitored either in the static regime or in the oscillating regime, respectively. Both detection methods have proved their suitability for biochemical sensing applications (8, 9). In the dynamic regime, cantilevers are both sensitive to mass loading and variation of surface elasticity induced by interacting target molecules (10). In many cases, gravimetric sensitivity is considered because its effect on the resonance frequency is well-known (11, 12). In contrast, the contribution of surface stress is often more ambiguous, as several models have been proposed (13-15), but they often mismatch experimental behavior in terms of sensitivity (16, 17). However, when transducers are used in liquid media, e.g., for biosensing applications, the cantilever mass sensitivity is significantly reduced due to viscous damping and fluid load effects, although the cantilevers remain very sensitive to surface stress as induced by target molecules and fluidic interactions (18, 19). Besides, in liquids, oscillating cantilevers offer much higher stability to external mechanical perturbations than they do in the static regime. Hence, it is crucial to consider cantilever stiffness sensitivity when operating these resonators in liquids.

For a given geometry, the higher Young's modulus of diamond enables higher resonance frequency and *Q*-factor than for other material structures, thus making it a material of choice for such applications in liquids. Furthermore, the carbon-terminated surface of diamond may be easily modified by covalent bonding of organic compounds used as sensitive layers. Several immobilization routes have been reported in the literature (18-24). Recently, a new way to functionalize diamond, based on the chemistry of amines, was developed and demonstrated: a molecule containing an amine group can be strongly attached in one step onto hydrogen-terminated diamond surfaces (25, 26). In this work, we used this novel grafting technique to attach carboxylic acid moieties on home-fabricated diamond microcantilevers (27). The

technique used aminocaproic acid on the hydrogen-terminated surface of several diamond cantilever beams, hence leading to the grafting of the carboxylated alkyl chains. The goal here is to investigate the influence of electrostatic repulsions occurring at the beam surfaces on the cantilever resonance frequency when protonating/deprotonating the grafted carboxylic acid terminations by cycling the pH in a wide range (from 3 to 12). Similar experiments using thiol-modified carboxylated alkyl chains grafted on gold-coated silicon cantilevers were achieved to investigate cantilever sensitivity over molecular electrostatic interactions in static regime (28). This method is particularly interesting for dynamic regime sensitivity, since the gain or loss of protons induces virtually no change in the effective mass of the cantilever, and observations of the frequency shifts can only be attributed to the change molecular interactions. Thus, this approach enables one to characterize the sensitivity of our resonant diamond microcantilevers over molecular surface interactions by correlating the cantilever response to the $-COO^-/-COOH$ ratio on the surface induced by pH changes.

EXPERIMENTAL SECTION

1. Diamond Microcantilever Fabrication.

Diamond cantilevers were fabricated following a process described earlier (27). In brief, this process involves the direct growth of diamond patterns in silicon molds prior to removal of the sacrificial molds to free the diamond beams. The diamond nanoparticle seeding is achieved selectively inside the molds using standard clean room patterning approaches, followed by diamond growth in a semi-industrial microwave plasma chemical vapor deposition (MPCVD) reactor (SEKI AX6500X), on 4 in. wafers. Here, all fabricated cantilevers have a length and width of 400 and 200 μm, respectively. The beams average thickness was 1.2 ± 0.2 μm, as measured using optical interferometry. Such cantilever geometry led in air to a resonance frequency of 20221.8 ± 3300 Hz, a stiffness coefficient of 1.32 ± 1.3 N m^{-1}, and a Q-factor of 175. This low value of the Q-factor is due to the fairly long length of the structure and matches the expected theoretical value. In fluid, Q-factor is mainly dominated by viscous damping, and it was estimated here using the model proposed by Sader (29). Viscous damping dominated *Q*-factor can be improved by increasing the cantilevers thickness, but then cantilevers' surface effects and therefore surface stress sensitivity would be lowered at the same time. So we found these geometrical parameters to be a good compromise. Also, it is important to mention that in our case the *Q*-factor remains much higher than when using other common materials such a silicon or silicon nitride to make the structure. For example, a *Q*-factor ratio of more than 6 was reported between identical polycrystalline diamond and silicon mechanical resonators in low-damping media (30). In damped media like in aqueous solutions, the Q-factor, mainly dominated by viscous damping, is proportional to the square root of the product $E\rho$, where E and ρ are the Young modulus and the volume mass of the material, respectively. For instance, for a given geometry, the cantilever would give a *Q*-factor value twice lower when silicon is used instead of diamond (31).

Before caproic acid immobilization, the fabricated cantilevers were treated in a H_2SO_4 : H_2O_2 (5:1) bath for 1 h to remove any eventual contamination from the cantilevers fabrication steps and to ensure a clean diamond surface. Then the diamond cantilever surfaces were hydrogenated at 923 K in hydrogen plasma for 20 min using a microwave power of 2200 W and a pressure of 25 mbar.

2. Cantilever Resonance Frequency Measurements.

Diamond microcantilevers were mounted in a liquid cell underneath which an external piezoelectric vibrator was placed to allow structure actuation through acoustic waves. The resonance frequencies were measured using Doppler laser interferometry in a Polytec setup. In this setup, a coherent laser source emitting in the 620-690 nm range passes through a beam splitter. Half of the beam is sent to the resonant cantilever surface, where it is reflected back to an interferometer (OFV511) and a demodulator (OFV3001), where the cantilever resonance frequency is extracted. The other half of the beam is directly sent to the interferometer for reference. This setup can detect vertical oscillations in the picometer range, while cantilevers excited by the piezoelectric cell exhibit an amplitude between tens to a hundred nanometers at their resonance frequency (in air or in liquid). Using a frequency span of 1 kHz and a number of FFT points of 1600, the frequency resolution of the setup was 625 mHz. All resonance frequency measurements were achieved at a room temperature of 20 ±1 °C. The measured relative humidity in the experimentation room was 45% ± 5%. Before the caproic acid grafting, the resonant frequency of each cantilever was measured systematically in air and in the 0.2 M phosphate buffer at pH 10 to determine the load per unit length applied by the fluid on the cantilever using eq 4.

3. Grafting Procedure.

Caproic acid was immobilized on the cantilever surface using a very novel grafting process described elsewhere in the case of aminated biotin and ferrocene (25). Phosphate buffer (0.2 M, 600 μL) at pH 10 was injected in the liquid cell containing the cantilever. Since the cantilever environment was changed from air to liquid, a stabilization step was necessary to ensure homogenization of the liquid cell temperature and the cantilever fluid interface, which could also have influenced the resonance frequency. During this step, the resonance frequency evolution was monitored until stabilization. It was also verified that a phosphate buffer volume replacement does not affect significantly the stability of the resonance frequency. For this task, 300 μL of phosphate buffer was replaced by the same volume of fresh solution, and then the resonance frequency value was compared to the value measured before solution replacement. Next, aminocaproic acid solution was prepared by dissolving an adequate amount of aminocaproic acid salts (provided by Sigma Aldrich) in the same potassium phosphate buffer solution used to check the cantilever resonance frequency stability in the liquid cell. For the grafting steps, 300 μL of phosphate buffer from the liquid cell was replaced by the same volume of aminocaproic acid solution. The aminocaproic acid concentrations in the cell were either 10, 100, or 800 μM. Again the cantilever resonance frequency trend was monitored after aminocaproic acid injection in the liquid cell until stabilization. After the grafting step, the cantilever, still in the liquid cell, was rinsed thoroughly with the fresh phosphate buffer solution used to prepare the aminocaproic acid solution. Finally, the liquid cell was filled up with 600 μL of fresh phosphate buffer solution and the resonance frequency was monitored to verify its stability over time after grafting.

4. pH Cycling.

pH in the liquid cell was changed using 0.2 M phosphate buffer prepared at different pH values in the range of 3 to 12. After each pH change, the cantilever resonance frequency was found to be stable at most 1 min after the phosphate buffer change, the time at which the measurement was

made. For each pH change, the liquid cell was rinsed three times with the new phosphate buffer at the desired pH. Using this protocol, it was verified by proton concentration calculation and using a pH probe that the liquid cell content is at the desired pH.

5. XPS Analysis.

X-ray photoelectron spectroscopy (XPS) analysis was carried out in order to investigate the immobilization of caproic acid on the cantilever surfaces. Our XPS setup is composed of a spectrometer fitted with a hemispherical analyzer. Photons are emitted from an AI Kα anode ($h\nu$ = 1486.6 eV) equipped with a monochromator (AI Kα fwhm 0.25 eV). For each analyzed surface, attention was paid to the evolution of the oxygen core level following the surface treatment applied. The binding energy scale was calibrated using the Au 4f 7/2 peak located at 84.0 eV (32). The provided O1s spectra (Figure 2b) have been corrected from the inelastic background using a Shirley function (33). For practical reasons, XPS analysis was performed on 1 × 1 cm^2 diamond samples having undergone the same post-treatments as the cantilevers. Four diamond surfaces, on which different treatments were applied, were analyzed. After their surface treatment, the different samples were immediately transferred to the ultrahigh vacuum (UHV) setup. Sample HD, used as reference, was treated by the surface acid cleaning followed by the 20-min hydrogenation step described above. The three other samples, named HD+TP10 min, HD+grafting10 min, and HD+pH_cycles, respectively, underwent the same initial acid cleaning and hydrogenation steps as the reference surface (HD) before additional surface treatments. Sample HD+TP10 min was dipped in 0.2 M phosphate buffer at pH 10 during 10 min to investigate the influence of the phosphate buffer used on the diamond surface termination. Sample HD+grafting10 min was dipped in the 800 μM aminocaproic acid solution dissolved in 0.2 M phosphate buffer at pH 10 during 10 min for grafting. Sample HD+pH_cycles underwent three pH cycles from pH 12 to 3.5 to check the influence of pH cycling on bare hydrogen-terminated diamond surface. After surface treatments, all samples were rinsed in DI water for 3 min to prevent the presence of any phosphate potassium salts on the surface after drying with argon.

THEORETICAL BASIS

In the following, the cantilever resonance frequency in air extracted from Euler–Bernoulli theory is given by eq 1

$$f_r^{\text{air}} = \frac{\lambda_i^2}{2\pi}\frac{t}{L^2}\sqrt{\frac{E^*}{12\rho}}\sqrt{1-\frac{1}{2Q^2}} = \frac{1}{2\pi}\sqrt{\frac{k^*}{m^*}} \qquad (1)$$

where λ_i is the eigenvalue of the eigenmode that satisfies $\cos(\lambda_i)\cosh(\lambda_i) = -1$ (for the first bending mode of a free end rectangular cantilever $\lambda_1 = 1.875$), L and t are the cantilever length and thickness respectively, E^* is the cantilever effective Young's modulus, ρ is the cantilever density, Q is the cantilever Q-factor in the given media, k^* is the cantilever effective stiffness coefficient ($k^* = E^*Wt^3/4L^3$), m^* is the effective mass of the cantilever, and W is the cantilever width. Derivated from eq 1, the relative cantilever resonance frequency change due to a variation of mass (Δm) and stiffness (Δk) can be expressed by eq 2

$$\frac{\Delta f_r^{air}}{f_r^{air}} \cong \left(\sqrt{\left(1 + \frac{4L^3\Delta k}{E^* W t^3}\right)} \times \sqrt{\left(1 - \frac{\Delta m}{m^*}\right)} \right) - 1 \quad (2)$$

Please note that in this equation, the *Q*-factor is supposed to be constant. When the cantilever operates in liquid, the load applied by the fluid on the cantilever has to be taken into account. The effect of fluid damping on the resonance was modeled by introducing the mass applied by the fluid on the cantilever per unit length (34). Using this model, the evolution of the resonance frequency in liquid following mass and bending stiffness variation becomes

$$\frac{\Delta f_r^{liq}}{f_r^{liq}} \cong \left(\sqrt{\left(1 + \frac{4L^3\Delta k}{E^* W t^3}\right)} \times \sqrt{\left(1 - \frac{\Delta m}{m^*\left(1 + \frac{uL}{m^*}\right)}\right)} \right) - 1 \quad (3)$$

In this equation, u is the mass per unit length applied by the fluid, which can be extracted from the ratio of the measured cantilever resonance frequency in air and in the liquid cell

$$\frac{f_r^{air}}{f_r^{liq}} = \sqrt{\left(1 + \frac{uL}{m^*}\right)} \times \sqrt{\frac{1 - \frac{1}{2(Q^{air})^2}}{1 - \frac{1}{2(Q^{liq})^2}}} \quad (4)$$

where Q^{air} and Q^{liq} are the quality factors measured in air and in liquid, respectively. In the following, the contribution of the *Q*-factors will be neglected, as the values are generally above 100 and 10 in air and in aqueous solution, respectively, implying a poor impact of the *Q*-factor in this calculation. Using these typical values, the relative error is inferior to 1% when *Q*-factors influence is neglected.

Equation 3 will be used in the following to extract variations of cantilever stiffness, which can be induced by surface stress changes. Surface stress arising from molecule immobilization on the cantilevers surface can be split into a strain-independent and a strain-dependent contributions, respectively (35, 36). A differential strain-independent surface stress between the two cantilever sides is responsible for the structure bending. In the resonating regime, the contribution of strain-independent surface stress is often modeled as an equivalent axial force applied on the cantilever neutral axis and an equivalent bending moment (13, 16, 37). The variation of the cantilever flexural rigidity can thus be described by eq 4, where $(EI)\tau$ and $(EI)o$ are the cantilever flexural rigidity with and without strain-independent surface stress, respectively and τ is the strain-independent surface stress. The relation between a rectangular shape cantilever stiffness coefficient k and EI is given by eq 6

$$(EI)^{\tau} = (EI)^{o}\left(1 + \frac{2\tau L^3}{\pi^2 (EI)^{o}}\right) \quad (5)$$

$$k = \frac{3EI}{L^3} \quad (6)$$

Although this modeling has been used to explain cantilevers' sensitivity over molecular interaction induced surface stress, it was questioned in recent publications (35, 36, 38) because it does not take into account cantilever stress relaxations capability. Moreover, it was shown that, when used in an appropriate way, classical one-dimensional beam theory predicts that cantilever stiffness is independent from strain-independent surface stress (35). Nevertheless, more recent publications suggest that if a three-dimensional model is considered, then strain-independent surface stress influences cantilever stiffness (38, 39). Others groups proposed that rather than strain-independent surface stress, strain-dependent surface stress influences cantilevers resonance frequency (35, 36, 40). The influence of this contribution upon the cantilever flexural rigidity can be described by eq 6 derived from one-dimensional beam theory, where $(EI)^b$ and $(EI)^o$ are the cantilever flexural rigidity with and without strain-dependent surface stress, respectively, and b_{top} and b_{bottom} are the strain-dependent surface stress on the top and the bottom surface of the cantilever, respectively.

$$(EI)^b = (EI)^o\left(1 + 3\frac{(b_{top} + b_{bottom})}{Et}\right) \qquad (7)$$

Equation 7 and recent models of strain-independent surface stress (38, 39) predict a weak sensitivity of microcantilevers upon surface stress variations. Indeed, values of surface stress induced by immobilized molecular interactions reported in the literature (40, 41) are generally in the range of some to several hundred millinewtons/meter. Such values used in both eq 7 and 1 would predict a relative resonance frequency of typically some ppm, only for silicon-derivative cantilevers. In the case of diamond cantilevers, eq 7 and the newest model of strain-independent surface stress would predict lower sensitivity as CVD-diamond features a very high Young modulus and a low Poisson coefficient (42). Indeed, it is inversely proportional to the Young modulus. Hence, the advantage of using diamond structures for their superior Q-factor in liquids may be negated by a lower sensitivity. However, in a large majority of experimental studies, much higher relative resonance frequency shift induced by biological/chemical species immobilization was reported than that predicted by eq 7. Generally, values of several thousands of ppm induced by tens to hundreds of millinewtons/meter surface stress range are reported. In the case of protonation/deprotonation of carboxylic acid functions, values of surface stress change of typically 15 mN m–1 were measured on cantilevers operating in the static regime (28).

By considering such a value of strain-dependent stress in the dynamic regime, eq 7 combined with eq 1 would predict a resonance frequency shift of 774 μHz only in the case of a 400 × 200 × 1 μm3 diamond cantilever. Such a frequency shift is too weak to be measured. By taking this value as the strain-independent surface stress, then a significant resonance frequency shift of 100 Hz can be calculated using formulas 4 and 1. However, such calculation is questioned in the literature. The newest model of strain-independent surface stress based on a three-dimensional model would rather predict resonance frequency of some millihertz. These considerations illustrate the evidence of a serious mismatch existing between theoretical predictions and experimental observation. This controversy needs to be solved for clear interpretations of cantilevers' response in an oscillating regime.

RESULTS AND DISCUSSION

1. Resonant Behavior upon Caproic Acid Immobilization

The typical resonant frequency trend after the different steps of the microcantilever functionalization process is summarized in Figure 1a for an aminocaproic acid preparation solution of 800 µM. A significant decrease of the resonance frequency of approximately 8.85 Hz was observed at the end of the first stabilization step in the 0.2 M phosphate buffer. This resonance frequency shift may correspond to temperature stabilization in the liquid cell, adsorption of dissolved salts from the buffer solution on the cantilever surface, (43) and surface stress stabilization at the cantilever–liquid interface. Throughout all our experiments, the average time required for stabilization was found to be 35 ± 12 min. After stabilization of the resonance frequency, a second stabilization step was carried out by replacing half of the phosphate buffer in the liquid cell by a fresh identical buffer, as indicated in the Experimental Section. At the end of the second stabilization, the resonance frequency shift was not significant and confirmed the stability of the resonance frequency baseline. Then the cantilever was exposed to the buffer solution containing aminocaproic acid. A significant increase of the resonance frequency was observed and reached approximately 13.5 Hz after stabilization. The observation of a positive resonance frequency shift during the grafting step suggests that the main contribution for this shift is related to the change of cantilever elasticity rather than a change of cantilever effective mass induced by caproic acid immobilization on the cantilever surface. After the grafting step, the cantilever, in the liquid cell, was rinsed thoroughly with the pH 10 phosphate buffer, and then the resonant frequency was monitored again in fresh buffer to verify the signal stability of the functionalized cantilever. Figure 1a shows that a weak decrease of the resonance frequency was measured at the end of these steps, illustrating the good stability of the new baseline after grafting. It suggests a strong bond between the caproic acid and the cantilever surface. The small decrease of the resonance frequency after grafting may arise from caproic acid rearrangement on the surface (44) or desorption of molecules from the cantilever surface.

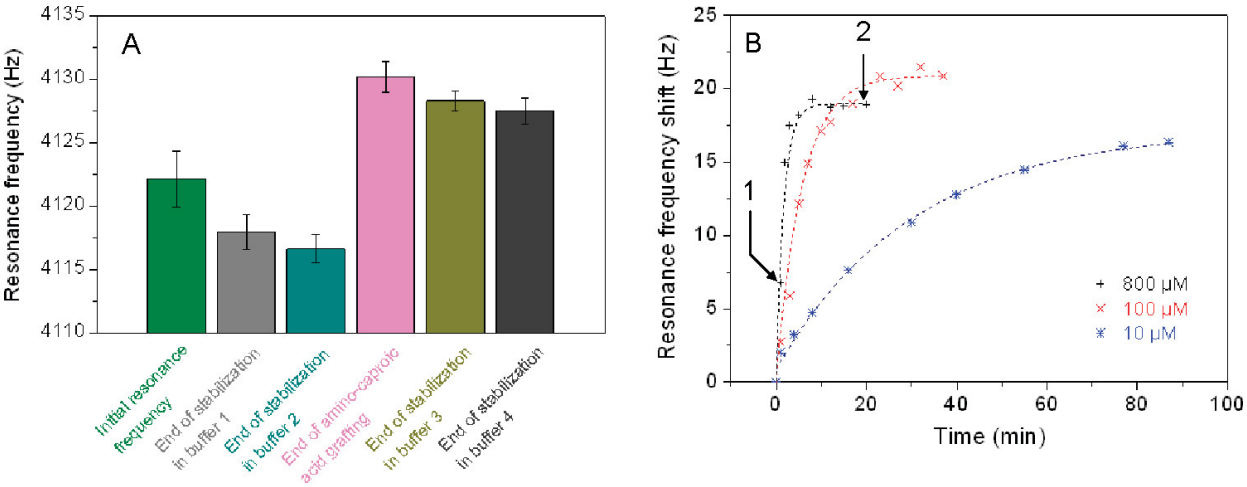

Figure 1. (a) Evolution of the resonance frequency of a cantilever at the end of the different grafting steps and (b) evolution of the resonance frequency versus time of three cantilevers during grafting step using 10, 100, and 800 µM concentrated aminocaproic acid solutions, respectively.

Figure 1b shows the evolution of the resonant frequency of diamond cantilevers during the grafting process when cantilevers are exposed to aminocaproic acid solution concentrations of 10, 100, and 800 μM. As expected, the grafting kinetics increases along with rising concentrations of aminocaproic acid. The time constants extracted by fitting a first-order exponential regression on the curves are 30.2, 5.6, and 2.7 min at 10, 100, and 800 μM, respectively. As expected, grafting time constant decreases when amino-caproic acid concentration increases, confirming that observed signal is linked to caproic acid immobilization on cantilevers surface. However, it seems that the time constants do not decrease linearly by increasing aminocaproic acid concentrations. Indeed, at too high values, physisorption is likely to occur and to superimpose to chemisorption due to the fact that at pH 10 carboxylic functions are deprotonated ($pK_a = 4.88$) and thus exhibit a negative charge while a significant proportion of amines ($pK_a = 11.3$) are protonated and hence show a positive charge. As a consequence, the greater the caproic acid coverage on the diamond surface, the more the negative charge of the grafted carboxylic functions on the diamond surface potentially attract $-NH_3^+$ functions of aminocaproic acid in solution, resulting in the observed rise of physisorbed species. Such a contribution of physisorption is likely to induce lower cantilever resonance frequencies as opposite to chemisorption, as it will be discussed later by considering cantilevers response over pH.

In a previous study, (25) ferrocene was grafted on hydrogen-terminated diamond using the same process. Attached ferrocene density was estimated to be in the range of 10–10 mol cm–2, corresponding to a compact monolayer. Here, if we consider that cantilevers response is affected only by electrostatic repulsion between $-COO^-$ terminations of a caproic acid monolayer, it is possible to assess the minimal density of grafted caproic acid by the calculation of the Debye length. Following this consideration, electrostatic repulsion would be negligible if the average distance between two adjacent immobilized $-COO^-$ terminations is much below the Debye length. Here, we considered electrostatic repulsions negligible if the average intermolecular distance is more than 5 times higher than the Debye length, because the magnitude of the electrostatic repulsions is often described to exponentially decrease with the ratio of the intermolecular distance onto the Debye length (45). In this case, we estimated the grafted caproic acid density to be at least equal to 2.8×10^{-11} mol cm^{-2} (1.6×10^{13} molecules/cm^2). This minored value of immobilized caproic acid is consistent with the density obtained in the case of ferrocene attachment (25).

2. XPS Analyses

XPS analysis was performed to characterize the diamond surfaces before and after caproic acid grafting. Figure 2a shows XPS survey spectra recorded on four different surfaces: HD, a bare hydrogenated diamond surface; HD+TP10 min, a bare hydrogenated diamond surface that was dipped in 0.2 M phosphate buffer at pH 10 for 10 min; HD+grafting10 min, an hydrogenated diamond surface exposed to an 800 μM aminocaproic acid solution for 10 min; and HD+pH_cycles, a bare hydrogenated diamond surface that was alternatively dipped three times in 0.2 M phosphate buffer at pH 12.5 and 3.5 for 5 min each. Figure 2b focuses on the oxygen core level (O1s) spectra of the four analyzed surfaces. The XPS spectra shown in Figure 2a,b are both normalized to the carbon C 1s peak.

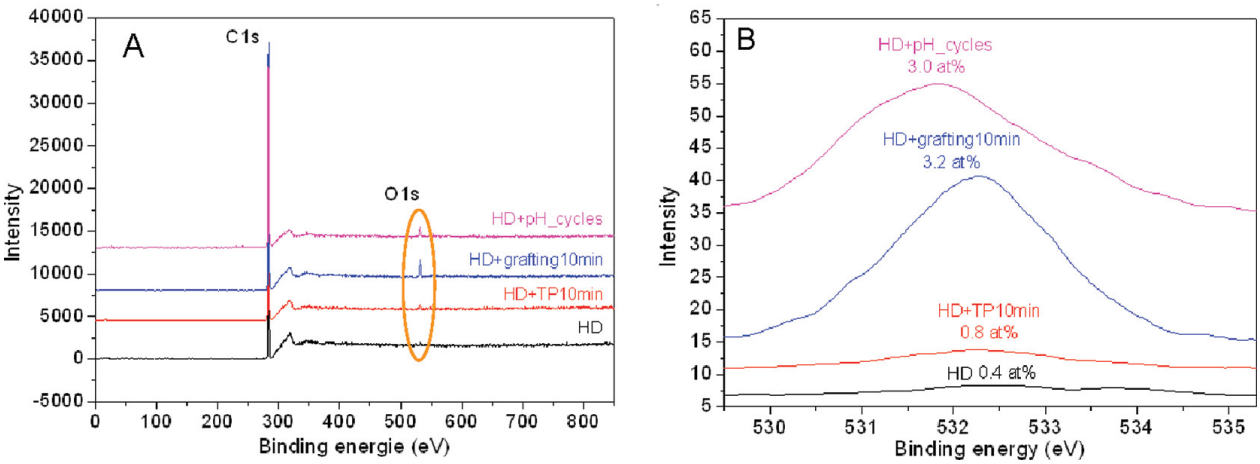

Figure 2. (a) Full XPS spectra and (b) oxygen core level spectra of four treated diamond surfaces. HD, bare hydrogenated diamond surface; HD+TP10 min, hydrogenated diamond surface that was immersed in 0.2 M phosphate buffer at pH 10 for 10 min; HD+grafting10 min, hydrogenated diamond surface that was exposed to aminocaproic acid for 10 min; and HD+pH_cycles, hydrogenated diamond surface that underwent three pH cycles.

Figure 2a reveals that the surface is mainly composed of carbon and oxygen. The main component of the carbon C1s signal arises from the diamond film. For all samples, the C1s peaks were located at 283.5 ± 0.2 eV and no significant change of the peak full width at half-maximum (fwhm) could be observed from one sample to another (0.8 eV). Consequently, C1s core level comparison between a bare diamond surface and a functionalized diamond surface is not trivial. Indeed, in our analysis, no significant change of the carbon core levels was observed between the four analyzed samples. In contrast, the comparison of oxygen core levels is more appropriate since carboxylic acid moieties from aminocaproic acid contain oxygen. Figure 2b shows that no oxygen is significantly present on the reference hydrogenated diamond surface as well as on the hydrogenated diamond surface that was dipped in phosphate buffer at pH 10 for 10 min. The oxygen atomic concentration between those two samples changed from 0.4 to 0.8 atom %. The very low value obtained for the hydrogenated diamond surface well-supports that contamination from air exposure can be neglected. Hence, it seems that dipping the hydrogen-terminated diamond surface into the buffer solution at pH 10 only does not significantly contribute to oxygen addition onto the surface. In contrast, when considering the functionalized surface, the oxygen concentration on the diamond surface increased from 0.4 to 3.2 atom % with respect to the bare hydrogenated diamond surface. Since the 0.2 M phosphate buffer at pH 10 does not seem to oxidize the diamond surface, it can be concluded here that the intensity of the oxygen peak is a result of the presence of caproic acid groups on the functionalized diamond surface. Finally, a significant amount of oxygen was found on the sample surface that underwent pH cycling from highly alkaline to highly acidic pH values, suggesting that as expected the diamond surface is oxidized when the surface is exposed to acidic pH values. Moreover, the oxygen peak (O1s) here is not located at the same binding energy than for the functionalized sample. This implies that the HD+pH_cycles (oxidized diamond surface) does not exhibit the same oxidized surface terminations as a caproic acid functionalized diamond surface. Nevertheless, surface evolution of a bare diamond cantilever from a hydrogen-terminated to oxide-terminated (C–OH, C–O–C, C═O, −COOH...) surface is likely to affect the surface energy and hence cantilever response but differently than a caproic acid functionalized cantilever. This will be discussed later.

Since aminocaproic acid contains an amine, nitrogen core level (N1s) was also investigated in an attempt to get some clues concerning the nature of amine-terminated molecules (here aminocaproic acid) linkage to diamond, which is still unknown (25). Two hypotheses can be formulated: either the molecule is attached to diamond through carbon–carbon covalent linkage or secondary amine function directly participates to the linkage. In the first hypothesis, no nitrogen is supposed to be detected while in that last case, nitrogen/oxygen stoichiometric proportions on hydrogenated diamond surface would be 1/2. This should be revealed by the XPS analysis. Here, a small amount of nitrogen was detected on the functionalized sample while no peak could be detected for all the other surfaces. The corresponding nitrogen surface concentration was found to be 0.3 atom %, which is 10 times smaller than the oxygen amount (3.2 atom %). This result does not fit with the expected nitrogen/oxygen stoichiometry of a monolayer linked to diamond via a secondary amine following the second hypothesis. Indeed, the quantity of nitrogen would be near twice lower than the quantity of oxygen instead of being 10 times smaller. Besides, the first hypothesis cannot be validated because the weak detected nitrogen amount may arise from physisorbed aminocaproic acid on the surface. This assumption will be considered later when analyzing the cantilevers response. Nevertheless, although the nature of caproic acid linkage can not be solved from this analysis, molecules linkage to diamond surface using this grafting method was found to be very strong (25).

3. Effect of pH on the Resonant Frequency

pH cycles were carried out on cantilevers having undertaken varying grafting durations in different aminocaproic acid solution concentrations. To start, we investigated the influence of the grafting duration at a given concentration. Cantilevers were grafted by dipping in a 800 μM concentrated aminocaproic acid solution for 1 or 30 min. As seen in Figure 1b, 1 min corresponds to the beginning of the grafting when the slope of the resonant frequency variation is high (indicated by label 1 in Figure 1b), and 30 min corresponds to a time when the resonant frequency has reached the plateau for several minutes (indicated by label 2 in Figure 1b). For each cantilever the response was recorded through several pH cycles in order to investigate the repeatability.

Parts a and b of Figure 3 show the resonance frequency behavior of both a bare hydrogenated diamond cantilever and a 1-min-grafted cantilever using 800 μM aminocaproic acid solution upon pH cycling.

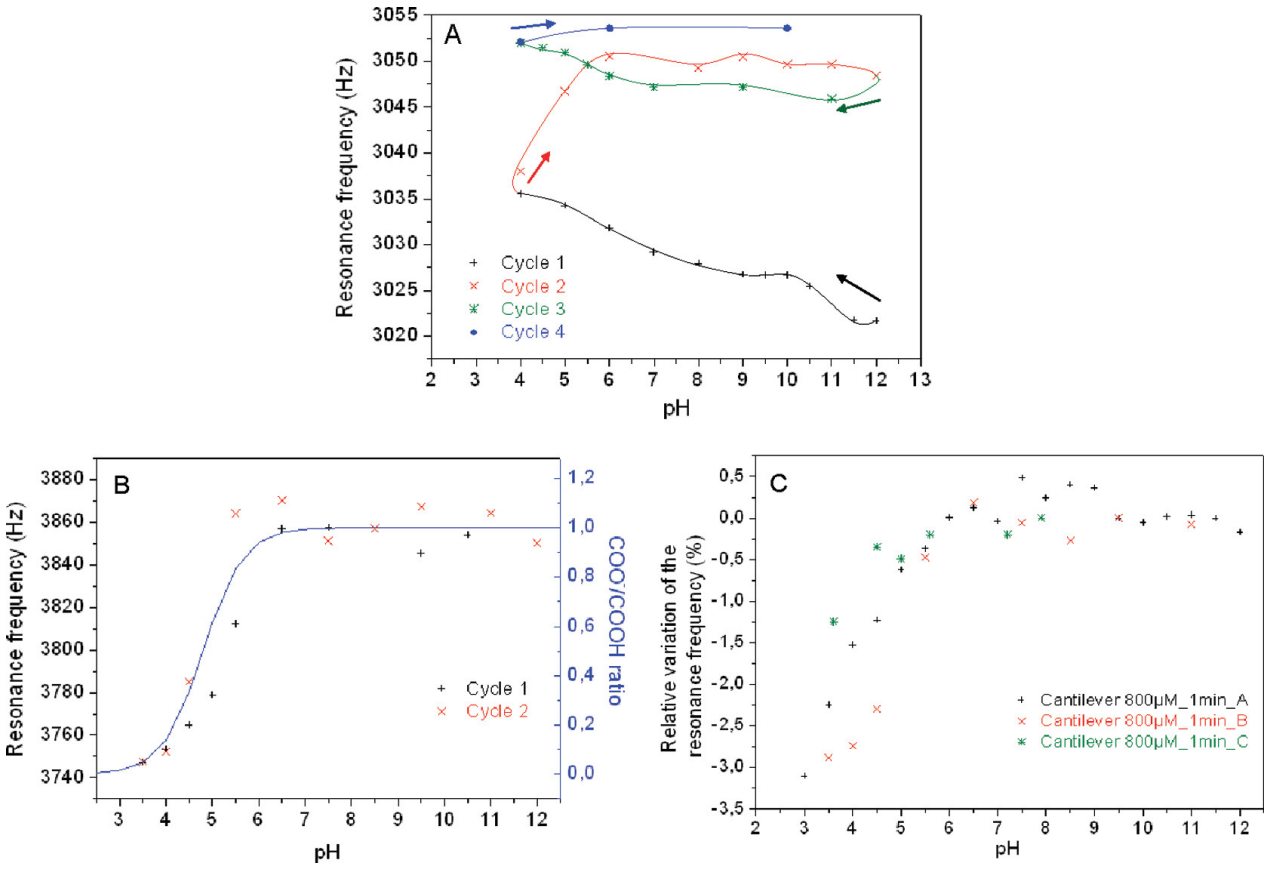

Figure 3. Resonance frequency responses of (a) a bare hydrogenated diamond cantilever following four pH cycles, (b) a 1-min-functionalized diamond cantilever with 800 µM aminocaproic acid solution following two pH cycles, (c) three 1-min-functionalized diamond cantilevers with 800 µM aminocaproic acid solution following pH.

An evolution of the bare diamond cantilever response was observed with respect to the number of pH cycles (Figure 3a). It was found that the resonance frequency significantly increases almost linearly from a pH of 12 to 4 during the first cycle and then tends to stabilize during the second cycle when pH values are increasing. Indeed, a plateau is observed from pH 6 during this second cycle. XPS analysis was carried out on a hydrogen-terminated diamond sample that was alternatively dipped three times in pH buffers from pH 12 to 3.5 and showed that its surface is significantly oxidized after such a treatment (Figure 2a). Hence, it is suggested that the bare diamond cantilever response trend is due to diamond surface oxidation occurring mainly in acidic media. After two pH cycles, diamond surface does not seem to evolve anymore with respect to the pH, as no significant resonance frequency shift was observed, confirming that the surface has reached a steady oxidation state.

Figure 3b shows that for the 1-min-dipped cantilever, a good overlap is observed between two curves corresponding to subsequent pH cycles, suggesting a good stability of the immobilized molecules on the cantilever surface. A significant decrease of the resonance frequency is observed when decreasing the pH, with a rapid drop of frequency starting to occur from around pH 5.5. Since the pKa value (46) of carboxylic acid functions of the aminocaproic acid is 4.88, it is reasonable to assume that from around the value of pH 5.5, the ratio of −COO–/–COOH starts to evolve significantly. Hence, it is suggested that, at a pH value above the carboxylic acid pKa,

charged −COO– terminations dominate and induce electrostatic repulsions that contribute to increase the cantilever bending stiffness. In the opposite case, carboxylic acid functions are protonated and −COOH terminations dominate. Consequently, electrostatic repulsions decrease when lowering the pH ,and van der Waals and hydrogen attraction between adjacent −COOH terminations may occur. (47) In this case, the cantilever bending stiffness significantly decreases.

In Figure 3b, an average resonance frequency shift of 109.2 ± 16.9 Hz was measured between the lowest pH value (pH 3.5) and the plateau (pH >5). Using eq 3, the corresponding cantilever stiffness variation was extracted. In the calculation, mass variation was neglected as here only protons are exchanged between immobilized carboxylic acid functions over the cantilever and the solution. As mentioned above, the density of immobilized molecules was estimated to be in the range of 1.3 × 10 (13) molecules cm–2, and if it is considered that every carboxylic acid termination are protonated/deprotonated at each pH cycles, then at most ±0.004 fg of proton would be exchanged with the cantilever surface (2 × 400 × 200 μm2). From eq 2, with $\Delta k = 0$, this would correspond to a relative resonance frequency variation of $\pm 1.65 \times 10^{-8}$% in air. In liquid, it was observed that the relative variation of the resonance frequency over mass is on average divided by 5 to 6 due to the load of the fluid on the cantilever, as modeled in eq 3 by the term (1 + uL/m*). This variation induced by the mass of adsorbed/desorbed protons is not measurable by our system, as the ideal frequency resolution is 625 mHz. Taking this in consideration, we now consider that the resonance frequency shift is only due to a variation of the cantilever stiffness. The resonance frequency shift measured here is very high when compared to theoretical predictions using eq 7. A variation of the cantilever stiffness of 123.7 ± 80.6 mN m–1 was calculated from measured resonance frequency shift by neglecting mass change contribution (Δm = 0 in eq 3). Young's modulus (E), length (L), width (W), and thickness of 980 GPa, 400 μm, 200 μm, and 1.4 μm, respectively, were taken for this calculation. The cantilever thickness was measured by interferometry as indicated in the experimental setup. For this cantilever, a resonance frequency of 23817 Hz was measured in air. This corresponds to a stiffness coefficient of 2.12 N m–1. Combining eqs 4 and 7 with eq 6, both equivalent strain-independent and strain-dependent surface stress variations were calculated from the value of cantilever stiffness variation (123.7 mN m^{-1}). Values of strain-independent and strain-dependent surface stress variations of 203.5 mN m^{-1} and 26 927.9 N m^{-1} were found, respectively. It is clear that the extracted value of strain-dependent surface stress variation has no physical sense. Inversely, the value of the strain-independent surface stress contribution found here is in good agreement with the values of surface stress reported in the literature (16). However, as mentioned in the Theoretical Basis, the influence of this contribution on the cantilever resonance frequency is still unclear and its calculation is questionable.

Another contribution affecting the cantilever resonance frequency may arise from the accumulation and the depletion of K^+, H^+, and phosphate ions of the buffer in the neighborhood of the cantilever, respectively, when grafted carboxylic acid functions are deprotoned. That would contribute to change locally the density of the fluid. In our case, it was assumed that the fluid density variation does not exceed 20 g L^{-1}, in the neighborhood of the cantilevers. Calculations using the Sader model (29) show that a 400 × 200 × 1.4 μm3 diamond cantilever has a sensitivity of 1.77 Hz/g/L over a change in fluid density. Hence, a variation of the local fluid density of at most ±35 Hz may be expected from this contribution, which is significant and thus might explain a part of the cantilever response to protonation/deprotonation.

Reproducibility was examined by repeating the 1-min-dipped experiment using a 800 µM aminocaproic acid solution three times on three different cantilevers having all identical dimensions. Figure 3c reveals that for each identical cantilever the same relative evolution of the resonance frequency versus pH was observed. This trend was directly fitted with the theoretical ratio of −COO–/–COOH terminations on the cantilever surface (figure 3c). A good correlation was observed between frequency variation and protonated/deprotonated acid ratio, strengthening the assumption that the cantilever stiffness is directly related to the amount of charges on the surface. Again, for these three cantilevers, diamond film thickness, resonance frequency in air, relative variation of the resonance frequency in phosphate buffer between the lowest pH value (pH 3.5) and the plateau (pH >5) respectively were measured to determine both cantilever initial stiffness and cantilever stiffness variation during pH cycles using eqs 1 and 3, if the variation of the resonance frequency is considered to be induced by a cantilever stiffness variation. The results are summarized in Table 1.

cantilever	**thickness (nm)**	**resonance frequency in air (Hz)**	**resonance frequency in liquid (Hz)**	**$[1 + (uL/m^*)]^{1/2}$**	***k* (N/m)**	**($\Delta f/f$) max in phosphate buffer (%)**	**Δk max in phosphate buffer (mN m^{-1})**
800u_1 min_A	1150	19418	3598.5	5.4	1.15	3.1	72.8
800u_1 min_B	1400	23817	3747.2	6.3	2.12	2.88	123.7
800u_1 min_C	1450	24890	3789.5	6.6	2.39	1.25	60.2

Table 1. Summarizing of Cantilevers Maximal Resonance Frequency Relative Variation during pH Cycling

In this table are indicated cantilevers thickness measured by interferometry, cantilevers resonance frequency measured both in air and in 0.2 M phosphate buffer at pH 10, the coefficient relative to the fluid load applied on the immersed cantilevers, cantilevers stiffness coefficient calculated from measured resonance frequency in air, measured cantilevers maximal resonance frequency relative variation, and corresponding stiffness variation calculated by formula 3. The three cantilevers were functionalized with 800 µM aminocaproic acid solutions for 1 min.

The data shows as expected from theory that thicker cantilevers exhibit higher resonance frequencies in air as well as in liquid and that their resonance frequency in aqueous media is lower due to fluid load and damping. Both measured resonance frequency in air and in liquid allow the extraction of the dimensionless coefficient $[1+(uL/m^*)]^{1/2}$ relative to the influence of the fluid load applied on the cantilevers using formula 4. Although it seems that, in this case, the impact of the fluid load is related to the cantilever thickness, extracted values that were found between 5.4 and 6.6 are too close to confirm this trend. Furthermore, the relative cantilevers' resonance frequency between the lowest pH value (pH 3.5) and the plateau (pH >5) varies by several percents, corresponding to cantilevers stiffness variation of several tens of millinewtons/meter. This range of stiffness variation is in good agreement with some other experimental data reported in the literature (16, 37). The corresponding sensitivity over stiffness

variation was found to be 1.5 Hz mN^{-1} m for the 1150-nm-thick cantilever.

The resonant frequency change upon pH variations for the samples dipped in 800 µM caproic acid solution for 30 min is significantly different from that of the 1-min-dipped sample (Figures 4). Indeed, although the resonant frequency tends to decrease also below approximately a pH of 5.5, the frequency drop is typically 5 times lower than in the case of the 1-min-dipped sample. Furthermore, when increasing the pH value above pH 5.5 and up to pH 12, a plateau is not observed in contrast with the 1-min-dipped sample. Also, it can be seen that, for the 30-min-dipped sample, the cantilever response from pH 5.5 to 12 seems to evolve largely during the first pH cycle and then less during the further cycles. In this case, a repeatable response seems to be obtained from the second cycle onward (Figure 4).

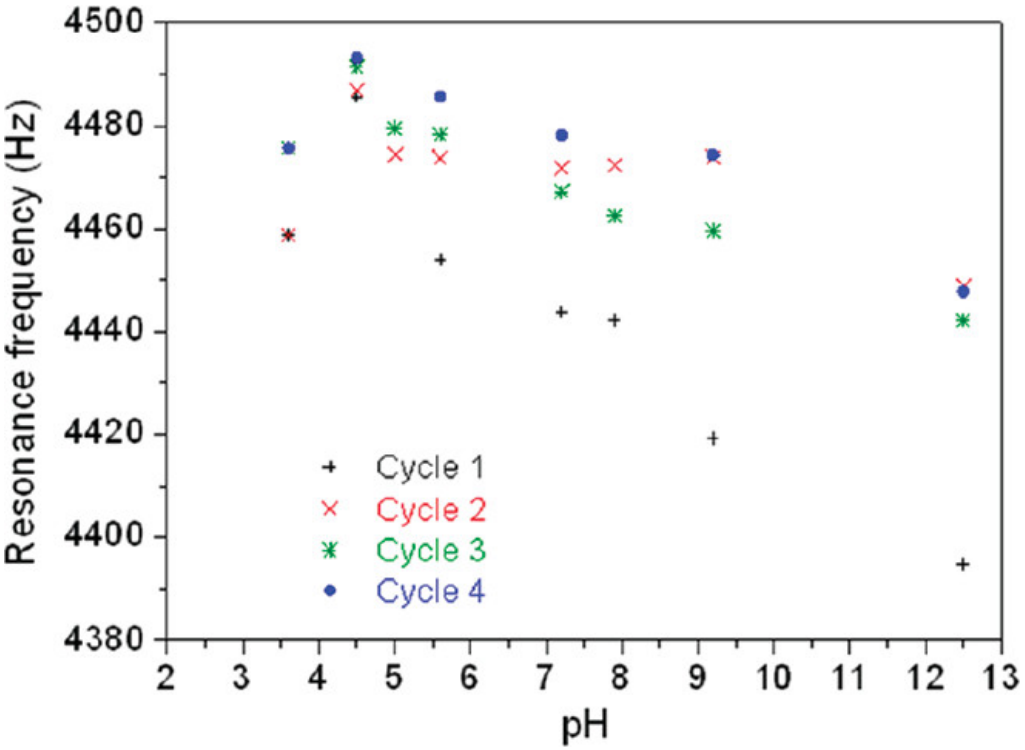

Figure 4. Resonance frequency responses of a 30-min-functionalized diamond cantilever with 800 µM aminocaproic acid solution following four pH cycles.

The same observation has been made when characterizing cantilevers grafted using 10 µM concentrated aminocaproic acid solution. When the grafting process was stopped before reaching a resonant frequency plateau, a good correlation was observed between frequency variation and protonated/deprotonated acid ratio. This was not the case for a cantilever left in aminocaproic solution long after the plateau was measured. This change of cantilever behavior between a short and a long grafting duration can be explained by a significant physisorption of aminocaproic acid that superimposes on chemisorption during the grafting step. Indeed, at grafting pH values (pH 10), some amines of the aminocaproic acid molecules are protonated and hence exhibit a positive charge, while the grafted carboxyl functions are deprotonated and consequently are negatively charged. So multilayer can be formed through ionic bonds and the longer the grafting duration, the higher the number of layers that could contribute in a different

manner than monolayer does. At the beginning of the grafting process, it is assumed that caproic acid is directly attached to the diamond surface, as reported (25) and suggested by XPS analysis (Figure 2a,b), thus forming the first layer. When caproic acid coverage increases with time, the ionic linkage rate of protonated amine to grafted $-COO^-$ terminations increases along with electrostatic attraction on the surface. In this way, during the formation of a new layer, the cantilevers resonance frequency may stabilize or decrease as, globally, negative charges cancel positive charges between two layers and because the average spacing between two charged carboxylic terminations increases during the formation of a new layer. When the new layer tends to be dense enough, then the average spacing between two charged carboxylic acid terminations decreases and again the resonance frequency increases. At the same time, the more aminocaproic acid adsorbed on the surface, the more attractive are van der Waals interactions between two CH chains, thus contributing to lower the resonance frequency. Such behavior may screen cantilever response over $-COO^-$ electrostatic repulsions when aminocaproic acid multilayers are deposited on cantilevers' surface. That would confirm the different cantilevers' response behavior. When the pH is cycling, protons may not easily reach the first caproic acid layer close to the diamond surface due to surface obstruction and charges effects. By considering that the ionic links are broken only on the first top layers due to carboxylic group protonation or amine deprotonation and considering that when the grafting is stopped early before resonance frequency stabilization, a quasi-monolayer is formed on the cantilever surface and the cantilever response over surface stress can be correlated to the evolution of the proportion of $-COO^-$ terminations. When the resonance frequency plateau is reached, multilayers are likely to be formed and thus will modify the cantilever response when cycling the pH. The latter case may explain the underestimation of nitrogen/oxygen stoichiometry measured by XPS. These two situations are represented in Figure 5.

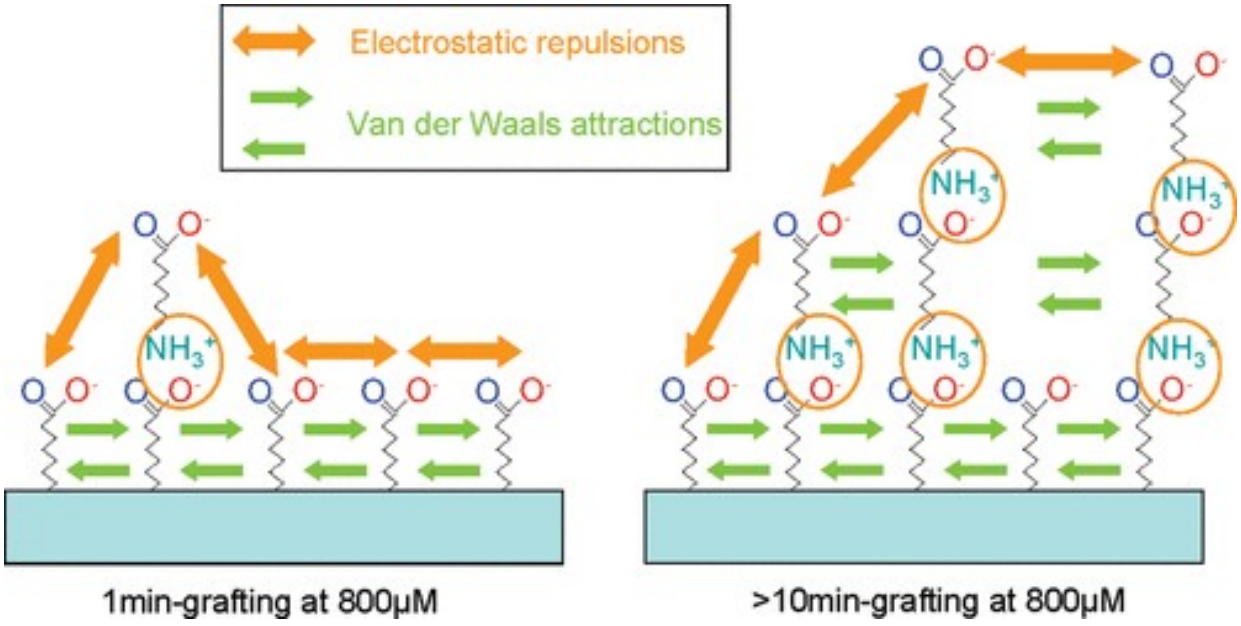

Figure 5. Illustration of cantilever surface configuration between a short and a long grafting

CONCLUSION

In this study, the sensitivity of diamond cantilevers over grafted molecular electrostatic interactions was experimentally studied by grafting carboxylic acid functions with aminocaproic acid. The presence of carboxylic acid functions on the diamond surface was confirmed by XPS analysis. By cycling the pH, two cantilever behaviors were observed following the cantilever grafting duration for a given concentration of aminocaproic acid. For a short grafting duration, a quasi-monolayer is supposed to be formed on the cantilever surface and an evolution of the proportion of carboxylic acid terminations can be correlated with the cantilever resonance frequency shift. Cantilever resonance frequency shift values as high as 109.2 ± 15.6 Hz induced by the change of molecular interaction regime was extracted. The resonance frequency shift observed here is very significant. Such magnitude is consistent with other experimental studies but mismatches recent theoretical predictions about the effect of surface stress upon cantilevers' resonance frequency. Thus, it is possible that other contributions like local change of fluid density induced by surface charges density variations influence the cantilever resonance frequency as well. In parallel, some effects of surface stress may be underestimated by theoretical predictions. For long grafting durations, the cantilever resonance frequency response variation suggests the presence of multilayers of aminocaproic acid. In summary, these experiments have demonstrated that resonating diamond cantilevers can be used in liquid to probe molecular interactions on their surface. Comparable sensitivity to silicon-derivative cantilevers working in static regime was observed. However, in the oscillating regime, less parasitic signal like random cantilever deflection may disturb the transducer response. Such diamond microcantilevers in the oscillating regime offer various possibilities for biosensing applications since many biomolecules (DNA, antibodies, or proteins) exhibit charges. The sensing of surface effects can be resolved with much higher sensitivities than one would have expected from the sole variation of the mass of the species to detect.

REFERENCES

(1) Yang, S. M.;Chang,C.;Yin,T. I.; Kuo, P. L. Sens. Actuators B 2008, 130, 674–681.
(2) Biswal, S. L.; Raorane, D.; Chaiken, A.; Birecki, H.; Majumdar, A. Anal. Chem. 2006, 78, 7104–7109.
(3) Su, M.; Li, S.; Dravid, V. P. Appl. Phys. Lett. 2003, 82, 3524–3564.
(4) Gupta, A.; Akin, D.; Bashir, R. J. Vac. Sci. Technol. B 2004, 22, 2785–2791.
(5) Dhayal, B.; Henne, W. A.; Doorneweerd, D. D.; Reifenberger, R. G.; Low, P. S. J. Am. Chem. Soc. 2006, 128, 3716–3721.
(6) Campbell, G. A.; Uknalis, J.; Tu, S.-I.; Mutharasan, R. Biosens. Bioelectron. 2007, 22, 1296–1302.
(7) Gupta, A.; Akin, D.; Bashir, R. Appl. Phys. Lett. 2004, 84, 1976.
(8) Eom, K.; Park,H. S.; Yoon, D. S.; Kwon, T. Phys. Rep. 2011, 503, 115–163.
(9) Arlett, J. L.; Myers, E. B.; Roukes, M. L. Nat. Nanotechnol. 2011, 6, 203–15.
(10) Lavrik, N. V.; Sepaniak, M. J.; Datskos, P. G. Rev. Sci. Instrum. 2004, 75, 2229–2253.
(11) Ilic, B.; Craighead, H. G.; Krylov, S.; Senaratne, W.; Ober, C.; Neuzil, P. J. Appl. Phys. 2004, 95, 3694–3703.
(12) Maraldo,D.;Mutharasan,R. Sens. Actuators B 2008, 132, 140–148.
(13) Lu, P.; Shen, F.; O'Shea, S. L.; Lee, K. H.; Ng, T. Y. Mater. Phys. Mech. 2001, 4, 51–55.
(15) Ren, Q.; Zhao, Y.-P. Microsyst. Technol. 2004, 10, 307–314.

(16) Chen, G. Y.; Thundat, T.; Wachter, E. A.; Warmack, R. J. J. Appl. Phys. 1995, 77, 3618–3622.
(17) Tamayo, J.; Humphris, A. D. L.; Malloy, A. M.; Miles, M. J. Ultramicroscopy 2001, 86, 167–173.
(18) Hwang, K. S.; Eom, K.; Lee, J. H.; Chun, D. W.; Cha, B. H.; Yoon, D. S.; Kim, T. S. Appl. Phys. Lett. 2006, 89, 173905.
(19) Chen, G. Y.; Thundat, T.; Wachter, E. A.; Warmack, R. J. J. Appl. Phys. 1995, 77, 3618–3622.
(20) H€artl, A.; Schmich, E.; Garrido, J. A.; Hernando, J.; Catharino, S. C. R.; et al. Nat. Mater. 2004, 3, 736–742.
(21) Shin,D.;Rezek, B.;Tokuda,N.;Takeuchi,D.;Watanabe, H.; et al. Phys. Status Solidi B 2003, 235.
(22) Sun, B.; Baker, S. E.; Butler, J. E.; Kim, H.; Russell, J. N.; et al. Diamond Relat. Mater. 2007, 16, 1608–1615.
(23) Yang, N.; Uetsuka, H.; Watanabe, H.; Nakamura, T.; Nebel, C. E. Chem. Mater. 2007, 19, 2852–2859.
(24) Nebel, C. E.; Rezek, B.; Shin, D.; Uetsuka, H.; Yang, N. J. Phys. D: Appl. Phys. 2007, 40, 6443–6466.
(25) Agn_es, C.; Ruffinatto, S.; Delbarre, E.; Roget, A.; Arnault, J.-C.; Omn_es, F.; Mailley, P. Mater. Sci. Eng. 2010, 16, 012001.
(26) Agnes, C.; Ruffinatto, S.; Mailley, P.; Omn_es, F. French Patent F-0954542, 2009.
(27) Bongrain, A.; Scorsone, E.; Rousseau, L.; Lissorgues, G.; Gesset, C.; et al. J. Micromech. Microeng. 2009, 19, 074015.
(28) Watari,M.; Galbraith, J.; Lang, H.-P.; Sousa, M.;Hegner,M.; et al. J. Am. Chem. Soc. 2007, 129, 601–609.
(29) Sader, J. E. J. Appl. Phys. 1998, 84, 64–76.
(30) Wang, J.; Butler, J. E.; Feygelson, T.; Nguyen, C. T.-C. IEEE Int. Conf. Micro Electro Mech. Syst. 2004, 17, 641–644.
(31) Bongrain,A.; Scorsone, E.;Rousseau, L.; Lissorgues,G.; Bergonzo, P. Sens. Actuators, B 2011, 154, 142–149.
(32) Seah, M. P. Surf. Interface Anal. 1993, 20, 243–266.
(33) Shirley, D. A. Phys. Rev. B 1972, 5, 4709.
(34) Vancura, C.; Dufour, I.; Heinrich, S. M.; Josse, F.; Hierlemann, A. Sens. Actuators A 2008, 141, 43–51.
(35) Lu, P.; Lee, H.; Lu, C.; O'Shea, S. Phys. Rev. B 2005, 72, 1–5.
(36) Kim, S.; Kihm, K. D. Appl. Phys. Lett. 2008, 93, 8–10.
(37) McFarland, A. W.; Poggi, M.; Doyle, M. J.; Bottomley, L.; Colton, J. S. Appl. Phys. Lett. 2005, 87, 053505.
(38) Lachut, M.; Sader, J. Phys. Rev. Lett. 2007, 99, 1–4.
(39) Lachut, M.; Sader, J. Appl. Phys. Lett. 2008, 95, 193505.
(40) Godin, M.; Tabard-Cossa, V.; Miyahara, Y.; Monga, T.;Williams, P. J.; Beaulieu, L. Y.; Bruce Lennox, R.; Grutter, P. Nanotechnology 2010, 21, 75501.
(41) Shin, S.; Kim, J. P.; Sim, S. J.; Lee, J. Appl. Phys. Lett. 2008, 93, 102902.
(42) Klein, C.; Cardinale, F. Diamond Relat. Mater. 1993, 2, 918–923.
(43) Rijal, K.; Mutharasan, R. Sens. Actuators B 2007, 124, 237–244.
(44) Godin, M.; Tabard-Cossa, V.; Miyahara, Y.; Monga, T.; Williams, P. J.; et al. Nanotechnology 2010, 21, 075501.

(45) Strey, H. H.; Parsegian, V. A.; Podgornik, R. Phys. Rev. Lett. 1997, 78, 895–898.
(46) MacCleanDavis,M.; Paabo,M. J. Org. Chem. 1966, 31, 1804–1810.
(47) Vezenov,D.V.;Noy,A.;Rozsnyai, L. F.; Lieber,C.M. J.Am.Chem. Soc. 1997, 119, 2006–2015.